Sensor signal processing

Enhancing the Sensitivity of Wireless *LC* Sensors Using Time Modulation

Nanshu Wu, Yichong Ren, and Pai-Yen Chen

Department of Electrical, Computer Engineering, University of Illinois Chicago, Chicago, IL 60607 USA
**Graduate Student Member, IEEE*
***Senior Member, IEEE*

Manuscript received 1 October 2024; accepted 26 October 2024. Date of publication 29 October 2024; date of current version 14 November 2024.

Abstract—We present an exceptional point (EP)-based temporally modulated wireless passive sensor, surpassing partly the shortcomings of traditional sensor structures, such as energy-consuming, low sensitivity, and hard-to-integrate. For traditional sensors, those factors mentioned above restrict the scope of applications. To address these limitations, temporally modulated EPs are introduced into *LC* tank sensing topologies. Originating from quantum mechanics, EPs are characterized by the coalescence of a system's complex eigenvalues, leading to considerable frequency splitting in response to minor perturbations. In this letter, comprehensive simulation results validate the feasibility and enhanced performance of this approach, confirming its superiority over existing sensor technologies. The introduction of EP-based wireless sensors equipped with time modulation marks a significant advancement in the field, promising substantial improvements in the sensitivity and accuracy of wireless sensors for a variety of applications.

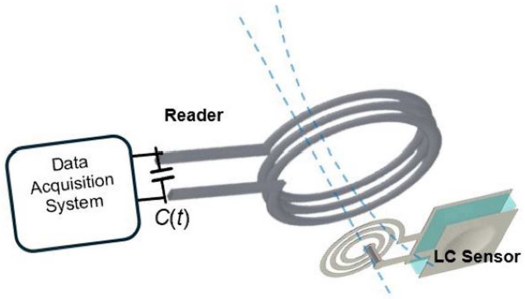

Index Terms—Sensor signal processing, exceptional points (EPs) degeneracy, time-modulation sensors, wireless sensors.

I. INTRODUCTION

Passive, maintenance-free wireless sensors have been extensively studied for various biomedical, industrial, automotive, and environmental applications [1], [2], [3], [4]. Typically, a wireless *LC* sensor consists of a coil antenna and a capacitive sensor or transducer, with its capacitance tuned by physical or (bio-)chemical quantities. Changes in the sensor's capacitance can be detected noninvasively by interrogating the passive sensor using a near-field coil antenna (via inductive coupling) and tracking the resonance frequency shift in the reflection spectrum. Improving sensitivity has always been a priority for researchers. Recently, exceptional point (EP)-based wireless *LC* sensors, which leverage eigenvalue bifurcations at an EP to enhance sensitivity, have emerged as a revolutionary class of sensor telemetry systems [5], [6]. EPs were first studied in parity-time ($\mathcal{PT}$)-symmetric non-Hermitian Hamiltonians in quantum mechanics and have since been experimentally observed in other classical systems such as optics, photonics, acoustics, and electronics [7], [8], [9]. In dispersion diagrams, EPs are where real eigenfrequencies begin to bifurcate (collapse) and imaginary eigenfrequencies collapse (bifurcate). This bifurcation in the energy space induces frequency splitting that is greater than what can be observed in traditional *LC*-based sensors, where EPs do not exist in the energy space. Researchers have found that sensors and telemetry systems with standard or higher order $\mathcal{PT}$-symmetric topologies exhibit significantly enhanced sensitivity in terms of resonance frequency shift due to the eigenvalue bifurcation induced by an EP [10], [11], [12]. However, the implementation of $\mathcal{PT}$-symmetric systems can be complicated by the use of active components, such as operational amplifiers, which can be unstable and noisy, thus limiting their potential in practical, ubiquitous wireless sensing applications. In addition, the $\mathcal{PT}$-symmetric sensing system requires a vector network analyzer for measurements, which is bulky and expensive, limiting the scope of potential applications. To facilitate the practice of EP-based sensing and telemetry, we here propose a time-modulated telemetry technique that enables the implementation of EP-based wireless sensing systems with reduced cost, simplicity, and low energy consumption, as illustrated in Fig. 1. In this telemetry system, the reader consisting of a coil antenna and a time-varying capacitor is used to wirelessly interrogate a general *LC* sensor using near-field inductive coupling. Perturbations in the sensor's capacitance result in a shift in resonance frequency. This can be obtained from the reflection spectrum recorded by an oscilloscope from reader part. Moreover, EP degeneracy in this time-modulated sensor telemetry system can significantly enhance sensitivity in terms of resonance frequency shift.

II. DESIGN PRINCIPLE

Fig. 1(a) depicts the proposed time-modulated wireless sensing system. On the sensor's side, a variable capacitor (e.g., a micromachine pressure/stress sensor [13] or chemically-reconfigured capacitive sensor [14]) with a capacitance of ΔC is parallel connected to a fixed capacitor ($C_0 = 200$ nF). The combined capacitor $C_0 + \Delta C$ is then connected to a coil antenna with self-inductance $L = 5$ μH. The equivalent circuit in Fig. 1(b) is generally used to describe a wireless passive *LC* sensor. One the reader side, a coil antenna with self-inductance $L = 5$ μH is connected to a time-varying capacitor,

Corresponding author: Pai-Yen Chen (e-mail: pychen@uic.edu).
Associate Editor: Dimitrie Popescu.
Digital Object Identifier 10.1109/LSENS.2024.3487777

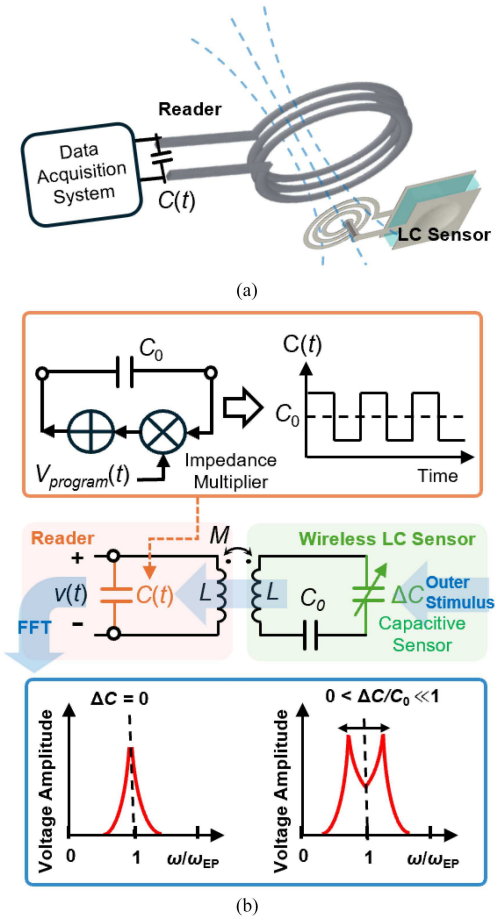

Fig. 1. (a) Schematic diagram and (b) practical implementation of the time-modulated telemetry sensing system with the EP-enhanced sensitivity.

whose capacitance follows a periodic piece-wise function:

$$\begin{cases} C(t) = (1-\zeta)C_0, & 0 < t \le T_1 \\ C(t) = (1+\zeta)C_0, & T_1 < t \le T_m \end{cases} \tag{1}$$

where T_m is the period of modulation, which corresponds to a modulation frequency $F_m = 1/T_m$. Here, we assume the average capacitance of $C(t)$ is C_0, based on which the actual capacitance value of $C(t)$ changes periodically over time. The modulation index $\zeta = 0.5$, $T_m = 3.827\mu$s, $T_1 = DT_m$ where $D = 0.5$ is the duty cycle, and the coupling coefficient between the reader coil and the sensor coil $\kappa = 0.8$. We note that duty cycle D is not optimized yet. Without applying the time modulation, the reader composed of a LC oscillator has an angular resonance frequency $\omega_0 = 1/\sqrt{LC_0}$. The inset of Fig. 1 illustrates the practical implementation of a time-modulated capacitor, of which a mixer (e.g., AD835, Analog Devices Inc.) is used to mimic the $C(t)$ under the control of ζ (also known as modulation depth), which can be either rectangular wave or sinusoidal wave with the period of T_m. Both duty cycle D and period of T_m along with the mixer manipulates the charge of C_0, in reader side, creating an equivalent time varying capacitance sharing the same duty cycle and period.

The time-modulated sensor telemetry system in Fig. 1 can be described by the state matrix $\underline{\mathbf{M}}(t)$ that relates the charge on the sensor and reader, $\mathbf{Q}_\mathrm{s}$ and $\mathbf{Q}_\mathrm{r}$, and the corresponding charge flows, $\dot{\mathbf{Q}}_\mathrm{s}$ and

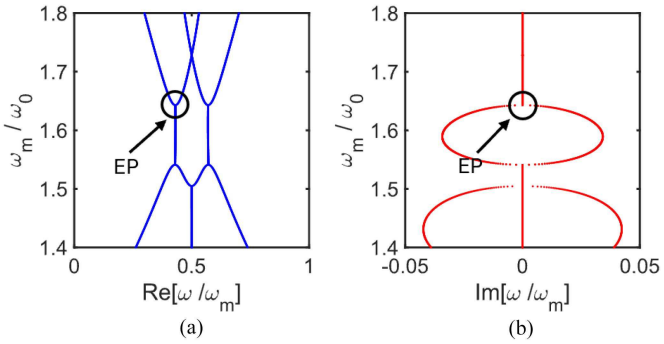

Fig. 2. Dispersion diagram of the (a) real part and (b) imaginary part of eigenfrequency for the time-modulated telemetry system in Fig. 1 with $\Delta C = 0$ (initial state); here, the modulation frequency $\omega_m/2\pi$ and eigenfrequency are normalized by the natural frequency ω_0.

$\dot{\mathbf{Q}}_\mathrm{r}$. From the Kirchhoffâs law, the state matrix can be derived as

$$\underline{\mathbf{M}}(t) = \begin{bmatrix} 0 & 0 & 1 & 0 \\ 0 & 0 & 0 & 1 \\ \frac{-1}{LC(t)(1-\kappa^2)} & \frac{\kappa}{LC_0(1-\kappa^2)} & 0 & 0 \\ \frac{\kappa}{LC(t)(1-\kappa^2)} & \frac{-1}{LC_0(1-\kappa^2)} & 0 & 0 \end{bmatrix} \tag{2}$$

with the eigenstate $\boldsymbol{\Psi}(t) = [\mathbf{Q}_\mathrm{r}, \mathbf{Q}_\mathrm{s}, \dot{\mathbf{Q}}_\mathrm{r}, \dot{\mathbf{Q}}_\mathrm{s}]^\mathrm{T}$, forming a relation $\frac{\mathrm{d}\boldsymbol{\Psi}(t)}{\mathrm{d}t} = \underline{\mathbf{M}}(t)\boldsymbol{\Psi}(t)$. Considering the time-periodic modulation, the relation between $\boldsymbol{\Psi}(t+T_m)$ and $\boldsymbol{\Psi}(t)$ can be written as

$$\boldsymbol{\Psi}(t+T_m) = e^{i\omega T_m}\boldsymbol{\Psi}(t) \tag{3}$$

which accounts for Floquet harmonics associated to periodicity in time. Further, the state vector evolution from t to $t+T_m$ can be described by the state transition matrix $\underline{\boldsymbol{\Phi}}$

$$\boldsymbol{\Psi}(t, t+T_m) = \underline{\boldsymbol{\Phi}}(t, t+T_m)\,\boldsymbol{\Psi}(t). \tag{4}$$

Combing (3) and (4) leads to

$$\underline{\boldsymbol{\Phi}}(t, t+T_m)\,\boldsymbol{\Psi}(t) = \lambda\boldsymbol{\Psi}(t) \tag{5}$$

where $\lambda = e^{i\omega T_m}$ and $\boldsymbol{\Psi}(t)$ are eigenvalues and eigenvectors of $\underline{\boldsymbol{\Phi}}$, respectively. The eigenvalue and eigenfrequencies ($\omega = -i\frac{\ln(\lambda)}{T_m}$) can be obtained by letting $|\underline{\boldsymbol{\Phi}} - \lambda\underline{\mathbf{I}}| = 0$ [15].

Fig. 2 presents the calculated dispersion diagram of time-modulated telemetry system with $\Delta C = 0$. As can be seen in Fig. 2, there are multiple EPs: branch points in the eigenspectrum. For example, an EP highlighted with a circle is at $\omega_{m,\mathrm{EP}} = 1.642\omega_0$ ($\omega_0/2\pi = 159.155$ kHz). When the system operates exactly at the EP, the real parts of the eigenfrequencies coalesce while the imaginary parts become zero, leading to a linear growth or decay of voltage across the capacitor over time. When a proper perturbation is applied, the coalesced eigenfrequencies split into two distinct real eigenfrequencies in a drastic bifurcation near the EP. This effect can be leveraged to enhance the sensitivity of passive LC wireless sensors, following the relationship $\lambda_p(\varepsilon) \propto \sqrt[n]{\varepsilon}$, where $\lambda_p(\varepsilon)$ represents the perturbed eigenvalue of the system, n is the order of the sensing system, and ε refers to the perturbation. This nth-square-root behavior described here can be used to significantly enhance the sensitivity of wireless readout sensors.

III. MODEL VERIFICATION

The equivalent circuit of the time-modulated telemetric sensing system in Fig. 1 was simulated using keysight advanced design system [16]. At $t = 0$, the circuit is excited by a voltage pulse with the amplitude of 50 mV, and changes in voltage across the reader's

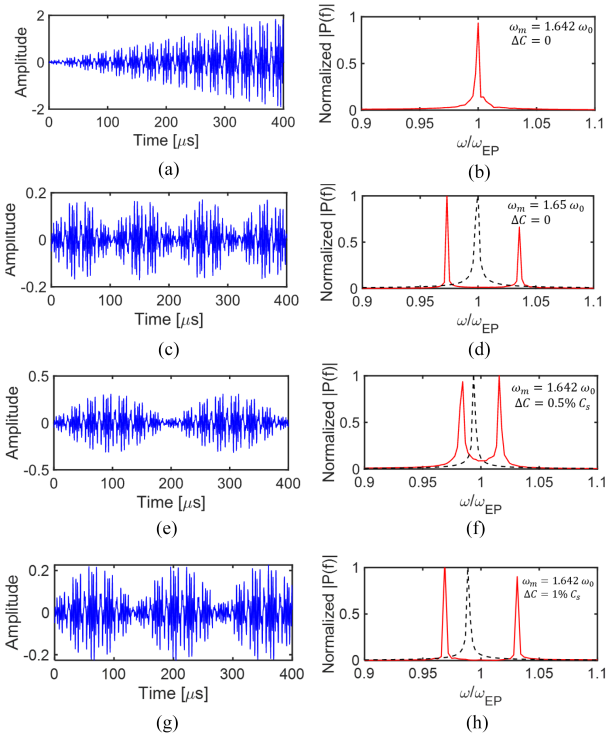

Fig. 3. (a) Transient response and (b) corresponding spectral analysis of the time-modulated telemetry system at the EP ($\omega_{m,EP} = 1.642\omega_0$) without perturbation ($\Delta C = 0$). (c) and (d) are similar to (a) and (b) but at a higher modulation frequency ($\omega_m = 1.65\omega_0$). (e) and (f) are similar to (a) and (b) but with a small capacitive perturbation ($\Delta C = 0.5\,\%C_0$). (g) and (h) refer to the transient response and spectral analysis at the EP ($\omega_{m,\mathrm{EP}} = 1.642\omega_0$) with perturbation ($\Delta C = 1\,\%C_0$). The black dashed lines in (d), (f), and (h) represent frequency shifts without time modulation for each corresponding perturbation.

capacitor over time are recorded. Fig. 3(a) reports the transient voltage response at the modulation frequency $\omega_{m,EP}/2\pi = 261.465$ kHz, displaying a linearly ascending oscillation [17], along with a single sharp tone in the frequency spectrum, as obtained via fast Fourier transform (FFT), shown in Fig. 3(b), consistent with the dispersion diagram in Fig. 2. Fig. 3(c) report the transient and spectral responses of the same time-modulated circuit at $\omega_m = 1.65\omega_0(1.005\omega_{m,\mathrm{EP}})$. It can be seen from Fig. 3(d) that when the modulation frequency ω_m increases slightly away from the EP, the resonant peak will bifurcate into two different peaks, as can be understood from Fig. 2. Fig. 3(e) reports that the transient and spectral responses at $\omega_{m,\mathrm{EP}}$, under a 0.5 % change in the sensor's capacitance (i.e., $\Delta C = 0.5\,\%C_0$). It can be seen from Fig. 3(f) that that the resonant peak splits into $\omega_1 = 0.984\omega_{m,\mathrm{EP}}$ and $\omega_2 = 1.016\omega_{m,\mathrm{EP}}$, corresponding to around a 3.20 % shift in the resonance frequency. When $\Delta C = 1\,\%C_0$, the time-modulation equipped sensing system is able to generate a bifurcation of $\omega_1 = 0.969\omega_{m,\mathrm{EP}}$ and $\omega_2 = 1.031\omega_{m,\mathrm{EP}}$, providing a 6.20 % frequency splitting, with the corresponding time domain and frequency domain information shown in Fig. 3(g) and (h). Fig. 4 compares the resonance frequency shift obtained with the time-modulated telemetry method and traditional time-invariant (i.e., a static capacitor is used on the reader) counterpart, under the same small-scale capacitive perturbations. It is evident that the resonance frequency shift can be enhanced substantially by adopting the time-modulated readout circuit, which potentially enables ultrasensitive and ultrahigh-resolution wireless sensing and telemetering. We note that the sensitivity may be further enhanced through optimization of the modulation depth/shape and duty cycle.

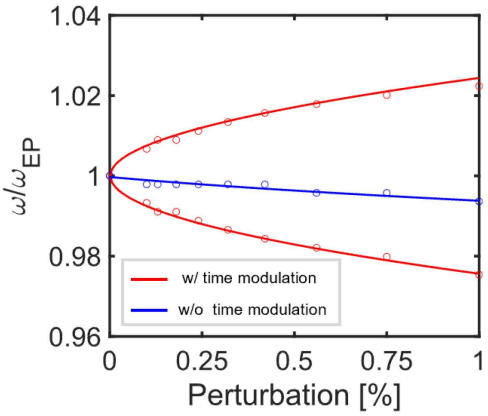

Fig. 4. Resonance frequency shift as a function of capacitive perturbation obtained with (red lines) and without (blue line) time modulation applied to the reader circuit; lines and dots represent analytical and numerical results, respectively.

IV. SENSITIVITY LIMITATION ANALYSIS

To explore the physical sensitivity limitations, we must first analyze the bifurcation process in the proposed telemetry system when subjected to a small perturbation ε. When the perturbation ε is applied to the system, the state transition matrix $\underline{\mathbf{\Phi}}$ changes, resulting in alterations to all related eigenvalues $\lambda_h(\varepsilon)$ ($h = 0, 1, 2, 3$, referring to different eigenvalues). This leads to a strong bifurcation in the frequency domain around the EP resonance frequency. Here, we employ the Puiseux series [18] to represent these perturbed eigenvalues. The first order of the equivalent eigenvalues for our proposed model is formulated as

$$\lambda_h(\varepsilon) \approx \lambda_0 + (i)^h \alpha_1(\varepsilon)^{\frac{1}{4}} \tag{6}$$

where λ_0 is the unperturbed eigenvalue, $\lambda_h(\varepsilon)$ represents all the disturbed eigenvalues with $h = 0, 1, 2, 3$ respectively for the fourth-order non-Hermitian system, the coefficient α_1 is expressed as

$$\alpha_1 = \left(-\frac{\frac{\partial f}{\partial \varepsilon}(\varepsilon, \lambda)}{\frac{1}{4!}\frac{\partial^4 f}{\partial \lambda^4}(\varepsilon, \lambda)} \right)^{1/4} \Bigg|_{\varepsilon=0, \lambda=\lambda_0} \tag{7}$$

where $f(\varepsilon, \lambda) = \det[\underline{\mathbf{\Phi}}(\varepsilon) - \lambda \underline{\mathbf{I}}]$. Deriving analytical expressions for perturbed eigenvalues is challenging for two reasons: first, there is no determined analytical solution for the eigenvalues of a 4×4 matrix; second, the analytical solution for the fourth-order derivative $\frac{\partial^4 f}{\partial \lambda^4}(\varepsilon, \lambda)$ is complex due to uncertainties in solving the eigenvalues. Therefore, we directly seek numerical solutions for (6) and (7). To simplify calculations, we use the central difference approximation method to approximate $\frac{\partial^4 f}{\partial \lambda^4}(\varepsilon, \lambda)$. We first evaluate how different combinations of L and C_0 will affect the system's sensitivity when the LC_0 product is constant ($LC_0 = 1 \times 10^{-12}$ s^2). We assess the frequency splitting of the system under a 1 % perturbation, shown in Fig. 5(a). It is observed that when LC_0 remains constant, the frequency splitting rate is unaffected by different pairings of C_0 and L, maintaining around 5.19 %. Although the trend of sensitivity limits cannot be detected from this aspect, it is still helpful for future system design. In practice, the accuracy of capacitors or inductors varies across different value ranges. We can adjust the L and C_0 combinations according to different testing scenarios to achieve optimal performance without affecting system sensitivity.

Having analyzed the impact of different LC_0 setups on sensing sensitivity, we next explore the impact of two variables related to

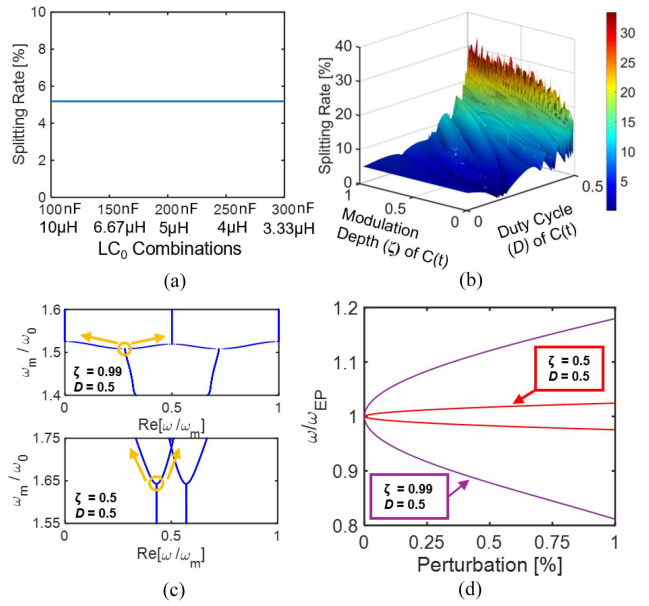

Fig. 5. Splitting rates under a $\Delta C = 1\,\%C_0$ perturbation for (a) different LC_0 combinations with $LC_0 = 1 \times 10^{-12}$ s^2 and (b) different modulation depths ζ and duty cycles D of $C(t)$. (c) Dispersion diagram for $\zeta = 0.99$ and $\zeta = 0.5$ and (d) frequency bifurcation diagram for $\zeta = 0.99$ and $\zeta = 0.5$.

$C(t)$ on system sensitivity: modulation depth ζ and duty cycle D. Modulation depth ζ, set to 0.5 by default, describes the difference in capacitance values between the maximum and minimum values of $C(t)$ within T_m. Typically, ζ ranges between 0 and 1. When ζ is near 0, the maximum and minimum values of $C(t)$ will approach C_0, and when ζ is near 1, they approach $2C_0$. We sweep ζ from 0.01 to 0.99. The duty cycle of $C(t)$, represented by D, theoretically ranges from 0 to 1, but practical consideration limits it to 0.5, as higher values eliminate temporal changes, undermining sensitivity.

The numerical results of the proposed sensing system's splitting rate over ζ and D are depicted in Fig. 5(b). The splitting rate increases with the D, and regardless of ζ, the maximum splitting rate occurs at the D of 0.5, indicating that a balanced duty cycle is essential for high sensitivity. When examining different duty cycles, we observe that, in general, the frequency splitting rate shows an increasing trend with the increase of ζ. Within the given parameter range, the time-modulated telemetry system can reach a splitting rate of approximately 33.28 %. Fig. 5(c) depicts the dispersion diagram of eigenfrequencies for cases where $\zeta = 0.5$ and $\zeta = 0.99$. It is evident that increasing ζ significantly enhances the bifurcation around the EP in energy space, as marked by orange arrows. The corresponding frequency splitting predictions are shown in Fig. 5(d), where a significant sensitivity enhancement to 36.85 % is achieved as ζ increases to 0.99. We emphasize that, in ideal cases, when $\zeta \to 1$, the sensitivity could become extremely high under a 1 % perturbation. However, operating at extreme values of ζ may cause the telemetry system to malfunction due to experimental impracticalities. Noise is another factor that can undermine sensor performance. Fortunately, in our setup, the effect of noise can be mitigated by separating the reader from the sensor and performing post-calibration after installation, which will also help improve accuracy. That said, we acknowledge that operating in harsh environments will likely result in some loss of sensitivity, so finding the appropriate tradeoff between robustness and sensitivity is essential.

V. CONCLUSION

In this letter, we introduce the concept of a time-modulated telemetric sensing system that exploits EP-induced eigenfrequency bifurcations to enable ultrasensitive detection of small perturbations on a passive *LC* sensor. We theoretically investigate and numerically validate the proposed sensing framework, evaluating its physical sensitivity limitations under a 1 % perturbation. Our findings may unlock the potential of EP-based sensors for detecting subtle changes, such as crack detection, microfluidics sensing, and other high-precision applications, due to their high sensitivity, segmented deployment, flexibility in adjustments, and simple structures compared to traditional sensors. This could significantly contribute to the development of next-generation near-field communication-based wireless sensing systems.

ACKNOWLEDGMENT

This work was supported by NSF under Grant 2229659.
The authors would like to thank Xuecong Nie for the fruitful discussions.

REFERENCES

[1] B. Lin, Q. Tan, G. Zhang, L. Zhang, Y. Wang, and J. Xiong, "Temperature and pressure composite measurement system based on wireless passive lc sensor," *IEEE Trans. Instrum. Meas.*, vol. 70, 2021, Art. no. 9502811.
[2] T. He et al., "Mxene/sno2 heterojunction based chemical gas sensors," *Sensors Actuators B: Chem.*, vol. 329, 2021, Art. no. 129275.
[3] M. Lin, H. Hu, S. Zhou, and S. Xu, "Soft wearable devices for deep-tissue sensing," *Nature Rev. Mater.*, vol. 7, no. 11, pp. 850–869, 2022.
[4] Y. Ren, N. Wu, K.-C. Chang, Y.-S. Su, and P.-Y. Chen, "A zero-power harmonic tag for real-time wireless food quality monitoring," *IEEE Sens. Lett.*, vol. 8, no. 7, Jul. 2024, Art. no. 6007904.
[5] R. El-Ganainy, K. G. Makris, M. Khajavikhan, Z. H. Musslimani, S. Rotter, and D. N. Christodoulides, "Non-hermitian physics and pt symmetry," *Nature Phys.*, vol. 14, no. 1, pp. 11–19, 2018.
[6] A. Regensburger, C. Bersch, M.-A. Miri, G. Onishchukov, D. N. Christodoulides, and U. Peschel, "Parity–time synthetic photonic lattices," *Nature*, vol. 488, no. 7410, pp. 167–171, 2012.
[7] J. Y. Lee and P.-Y. Chen, "Optical forces and directionality in one-dimensional PT-symmetric photonics," *Phys. Rev. B*, vol. 104, no. 24, 2021, Art. no. 245426.
[8] Y. Meng et al., "Spinful topological phases in acoustic crystals with projective PT symmetry," *Phys. Rev. Lett.*, vol. 130, no. 2, 2023, Art. no. 26101.
[9] M. I. Rosa, M. Mazzotti, and M. Ruzzene, "Exceptional points and enhanced sensitivity in PT-symmetric continuous elastic media," *J. Mechan. Phys. Solids*, vol. 149, 2021, Art. no. 104325.
[10] Z. Ye, M. Yang, Y. Ren, C.-H. J. Hung, C.-T. M. Wu, and P.-Y. Chen, "Review on recent advances and applications of passive harmonic RFID systems," *IEEE J. Radio Freq. Identif.*, vol. 7, pp. 118–133, 2023.
[11] J. Wiersig, "Review of exceptional point-based sensors," *Photon. Res.*, vol. 8, no. 9, pp. 1457–1467, 2020.
[12] J. Yuan et al., "Exceptional points induced by time-varying mass to enhance the sensitivity of defect detection," *Phys. Rev. Appl.*, vol. 18, no. 6, 2022, Art. no. 64055.
[13] T. Li, H. Shang, B. Wang, C. Mao, and W. Wang, "High-pressure sensor with high sensitivity and high accuracy for full ocean depth measurements," *IEEE Sensors J.*, vol. 22, no. 5, pp. 3994–4003, Mar. 2022.
[14] P. K. Sharma et al., "Ultrasensitive and reusable graphene oxide-modified double-interdigitated capacitive (DIDC) sensing chip for detecting sars-cov-2," *ACS Sensors*, vol. 6, no. 9, pp. 3468–3476, 2021.
[15] H. Kazemi et al., "Ultra-sensitive radio frequency biosensor at an exceptional point of degeneracy induced by time modulation," *IEEE Sensors J.*, vol. 21, no. 6, pp. 7250–7259, Mar. 2021.
[16] Keysight, "Pathwave advanced design system," Jan. 2018. [Online]. Available: https://www.keysight.com/us/en/products/software/pathwave-design-software/pathwave-advanced-design-system.html
[17] H. Kazemi, M. Y. Nada, A. Nikzamir, F. Maddaleno, and F. Capolino, "Experimental demonstration of exceptional points of degeneracy in linear time periodic systems and exceptional sensitivity," *J. Appl. Phys.*, vol. 131, no. 14, 2022.
[18] A. Welters, "On explicit recursive formulas in the spectral perturbation analysis of a Jordan block," *SIAM J. Matrix Anal. Appl.*, vol. 32, no. 1, pp. 1–22, 2011.